JNT FACIT BUSINESS AND TECHNOLOGY JOURNAL
ISSN: 2526-4281 - ANO 2026 - MÊS DE MAIO
Ed. 74. Vol. 1 - Págs. 150-164
DOI: 10.5281/zenodo.20215180

CAPES

CNPq
Conselho Nacional de Desenvolvimento Científico e Tecnológico

QUALIS A2

INFLUENCE OF TOMOGRAPHIC ACQUISITION PROTOCOLS ON THE IDENTIFICATION OF PERI-IMPLANT BONE DEFECTS[1]

INTERFERÊNCIA DO PROTOCOLO DE AQUISIÇÃO TOMOGRÁFICA NA IDENTIFICAÇÃO DE DEFEITOS ÓSSEOS PERI-IMPLANTARES

Everton Naim MASSUD[2]
Division of Oral Radiology, São Leopoldo Mandic Faculty
São Leopoldo Mandic Research Institute
E-mail: evertonmassud@gmail.com
ORCID: http://orcid.org/0009-0002-0779-7414

Ariana de Oliveira Matuda MARTINS[2]
Division of Oral Radiology, São Leopoldo Mandic Faculty
São Leopoldo Mandic Research Institute
E-mail: arianamatuda2@gmail.com
ORCID: http://orcid.org/0009-0002-2876-1699

Gabriela Franco da Rosa CAETANO[3]
Division of Oral and Maxillofacial Radiology, Department of Stomatology
School of Dentistry, University of São Paulo, São Paulo (SP)
E-mail: gabrielafrc@usp.br
ORCID: http://orcid.org/0000-0002-4392-8402

Marcelo Gusmão Paraiso CAVALCANTI[3]
Division of Oral and Maxillofacial Radiology, Department of Stomatology
School of Dentistry, University of São Paulo, São Paulo (SP)
E-mail: mgpcaval@usp.br
ORCID: http://orcid.org/0000-0001-8011-9623

Mariana Quirino Silveira SOARES[2]
Division of Oral Radiology, São Leopoldo Mandic Faculty
São Leopoldo Mandic Research Institute
E-mail: mariana.soares@slmandic.edu.br
ORCID: http://orcid.org/0000-0002-9387-3729

Luiz Roberto Coutinho MANHÃES JÚNIOR[2]
Division of Oral Radiology, São Leopoldo Mandic Faculty
São Leopoldo Mandic Research Institute
E-mail: luiz.manhaes-junior@unesp.br
ORCID: http://orcid.org/0000-0003-1642-5241

[1] COMO CITAR: (ABNT): MASSUD, E. N.; MARTINS, A. O. M.; CAETANO, G. F. R.; CAVALCANTI, M. G. P.; SOARES, M. Q. S.; MANHÃES JÚNIOR, L. R. C. **JNT Facit Business and Technology Journal.** Qualis A2. ISSN: 2526-4281, Mês de Maio de 2026 - Ed. 74. VOL. 01. Págs. 150-164. Disponível: http://revistas.faculdadefacit.edu.br. Acesso em: ___/___/___.

[2] Division of Oral Radiology, São Leopoldo Mandic Faculty, São Leopoldo Mandic Research Institute, Campinas, São Paulo, Brazil

[3] Division of Oral and Maxillofacial Radiology, Department of Stomatology, School of Dentistry, University of São Paulo, São Paulo (SP), Brazil

ABSTRACT

Purpose: This study aimed to evaluate the influence of tomographic acquisition parameters (mAs and kV) from different devices on the identification and classification of peri-implant angular bone defects. **Material and methods:** Dental implants were placed in bovine ribs, and angular defects were surgically created in the cervical region of the implants using burs. Tomographic acquisitions were performed using two different CBCT devices (Accuitomo 170 and OP300). For each system, two distinct acquisition protocols were employed: Accuitomo 170 - ProtA1 (90kV, 8mA, 4x4 FOV) and ProtA2 (90kV, 7mA, 4x4 FOV); OP300 - ProtO1 (90kV, 12.5mA, 5x5 FOV) and ProtO2 (90kV, 6.3mA, 5x5 FOV). **Results:** The identification of peri-implant angular bone loss was satisfactory for both devices. ProtO1 and ProtO2 showed no significant difference in the identification of peri-implant angular bone defects. However, ProtA1 allowed for superior visualization of the types of peri-implant angular bone defects compared to ProtA2. **Conclusion:** It can be concluded that the tomographic acquisition protocol can directly interfere with the ability to identify the specific type of peri-implant angular bone defect.

Keywords: Cone-Beam Computed Tomography. Dental Implants. Alveolar Bone Loss. Radiation Dosage. Radiography. Dental.

Research conducted following approval by the Institutional Animal Care and Use Committee (IACUC) of the São Leopoldo Mandic School (CEUA SLMANDIC), protocol No. 2022/17.

INTRODUCTION

Radiographic imaging is essential for pre and postoperative evaluation of dental implants (Zhang et al, 2021). Peri-implant bone dehiscences may occur due to incorrect implant positioning, insufficient residual bone, excessive loading, and inflammatory processes (Sanz-Martin et al, 2020).

An accurate analysis of peri-implant bone defects supports implant maintenance and guides the appropriate treatment (Song et al, 2019). Due to its two-dimensional nature, periapical radiography presents superimpositions that may limit the visualization of anatomical structures on the buccal-lingual and buccal-palatal areas (Dave et al, 2013; Vadiati Saberi et al, 2019).

Cone-Beam Computed Tomography (CBCT) enables the exact localization of anatomical structures and the three-dimensional evaluation of bone loss and residual

bone (Akheshteh et al, 2020; Fienitz et al, 2012; Kuhl et al, 2016; Pinheiro et al, 2015). This imaging modality provides the necessary pre- and postoperative information for treatment success (Jalaluddin et al, 2024). In peri-implant bone defects, CBCT has demonstrated high diagnostic accuracy (Schriber et al, 2020), especially when compared to intraoral imaging, such as periapical radiography (Costa et al, 2023; Song et al., 2021), allowing for correct defect classification, measurement of depth and width, and visualization of the buccal and lingual/palatal areas (Song et al, 2021).

However, despite the numerous advantages of CBCT, artifacts caused by high-density objects, such as dental implants, affect image quality and impair visualization (Bayrak et al, 2020; Kamburoglu et al, 2013; Salemi et al, 2021). In the study conducted by Sawicki et al. (2022), it was observed that kilovoltage (kV), milliamperage (mA), and field of view (FOV) can influence the appearance of artifacts around dental implants. Simultaneously, Liedke et al. (2017) stated that the use of lower-resolution protocols increases the risk of failing to visualize the buccal area.

Therefore, this study aimed to evaluate the influence of tomographic acquisition factors (kV, mA, and FOV) from two different devices (Accuitomo 170 and OP300) on the identification and classification of peri-implant angular bone defects.

MATERIALS AND METHODS

Following cleaning and disinfection, 24 fresh bovine rib bone specimens were prepared into blocks approximately 4.00 cm in length to simulate the alveolar bone for implant insertion, as well as the creation of angular defects and bone dehiscences, according to the methodology described by Vadiati Saberi et al. (2019). For each one, a titanium implant (DentiFix, Brazil) of the same brand, shape, size (3.75 x 11.5 mm), and surface treatment was inserted at a 90° angle.

The 24 bone blocks were randomly assigned into two groups and kept refrigerated to prevent moisture loss between tomographic acquisitions: Control Group (CG, n=12) and Angular Bone Defect Group (BD, n=12). Angular bone defects were created using a #2 spherical diamond bur. During preparation, the bone adjacent to the osteotomies was selectively removed to produce angular defects. Each defect was standardized to a depth of 3 mm, which was verified with a millimeter periodontal probe, while the width corresponded to the diameter of the bur.

Bone defects (BD) were created based on the number of bone walls involved, ranging from one to four walls. Each type was reproduced three times within the BD group, resulting in three specimens with one-wall defects, three specimens with two-wall defects, three specimens with three-wall defects, and three specimens with four-

wall defects. Spherical diamond burs were used to prepare the bone defects, which were then coated with wax.

Tomographic acquisitions were performed using the following devices: Accuitomo 170 (Morita, Kyoto, Japan), referred to as Protocol A, and OP300 (Instrumentarium, Tuusula, Finland), referred to as Protocol O. From these systems, two acquisition protocols were selected for each, as follows:

Device	Protocol	Resolution	kV	mA	FOV
Accuitomo 170	ProtA1	High Resolution (HR)	90	8,0	4 x 4 cm
	ProtA2	Standard (STD)	90	7,0	4 x 4 cm
OP300	ProtO1	(Endodontic) ENDO	90	12,5	5 x 5 cm
	ProtO2	Standard (STD)	90	6,3	5 x 5 cm

All tomographic acquisitions were exported in DICOM format and submitted for evaluation using the OnDemand3D software (Cybermed, Korea). Image interpretation was performed by a radiologist with three years of experience. The 3D-MPR tool was utilized, allowing for the simultaneous analysis of multiplanar reconstructions (MPR) - axial, coronal, and sagital - as well as paraxial and circumferencial reconstructions without information loss. All tomographic acquisitions were evaluated randomly, blinded to the specimen number, group (CG or BD), and acquisition protocol. The observer was instructed to follow pre-defined scores and select a single response according to the diagram below:

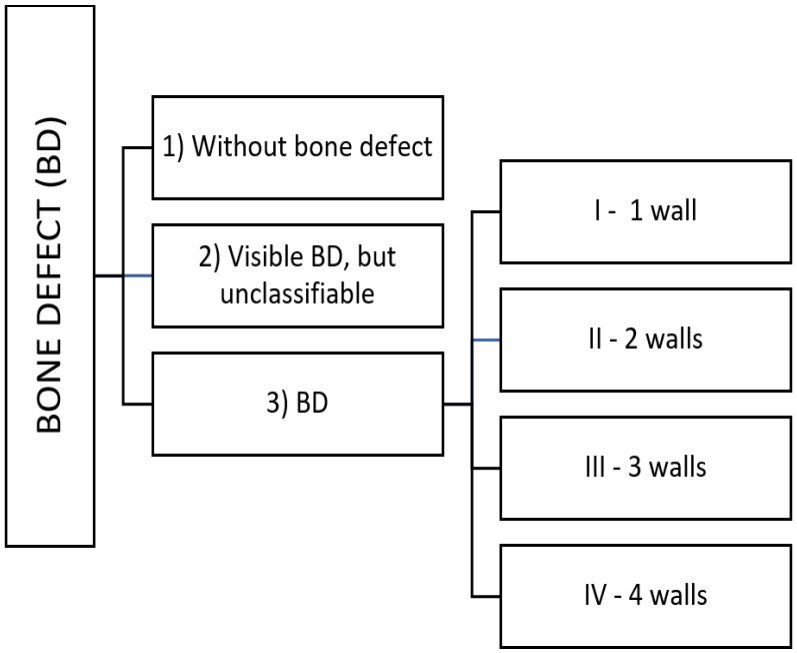

Figures 1–5 show multiplanar reconstructions (MPR) (axial, coronal, and sagittal) acquired with the Accuitomo 170 unit (Morita, Kyoto, Japan) with a high-resolution protocol (90 kVp; 8.0 mA; 4 × 4 cm FOV; 30.8 s acquisition time; 0.08-mm

voxel size), depicting 1-, 2-, 3-, and 4-wall bone defects, as well as sites without bone defects (control group). Unlabeled arrows indicate the bone defects.

Twenty percent of the sample was randomly re-evaluated twice within a 15-day interval, blinded to the specimens, to verify methodological replicability and reliability. To assess the reliability of the method, Cohen's Kappa coefficient was used, with 95% Confidence Intervals (95% CI) and the percentage of agreement between initial evaluations and re-evaluations. The results showed 94.8% agreement, representing a Kappa coefficient of 0.927 (95% CI: 0.865, 0.989), indicating excellent agreement and validating the reliability of the evaluation method.

Figure 1: Sagittal, axial, and coronal reconstructions of the control group (without bone defects).

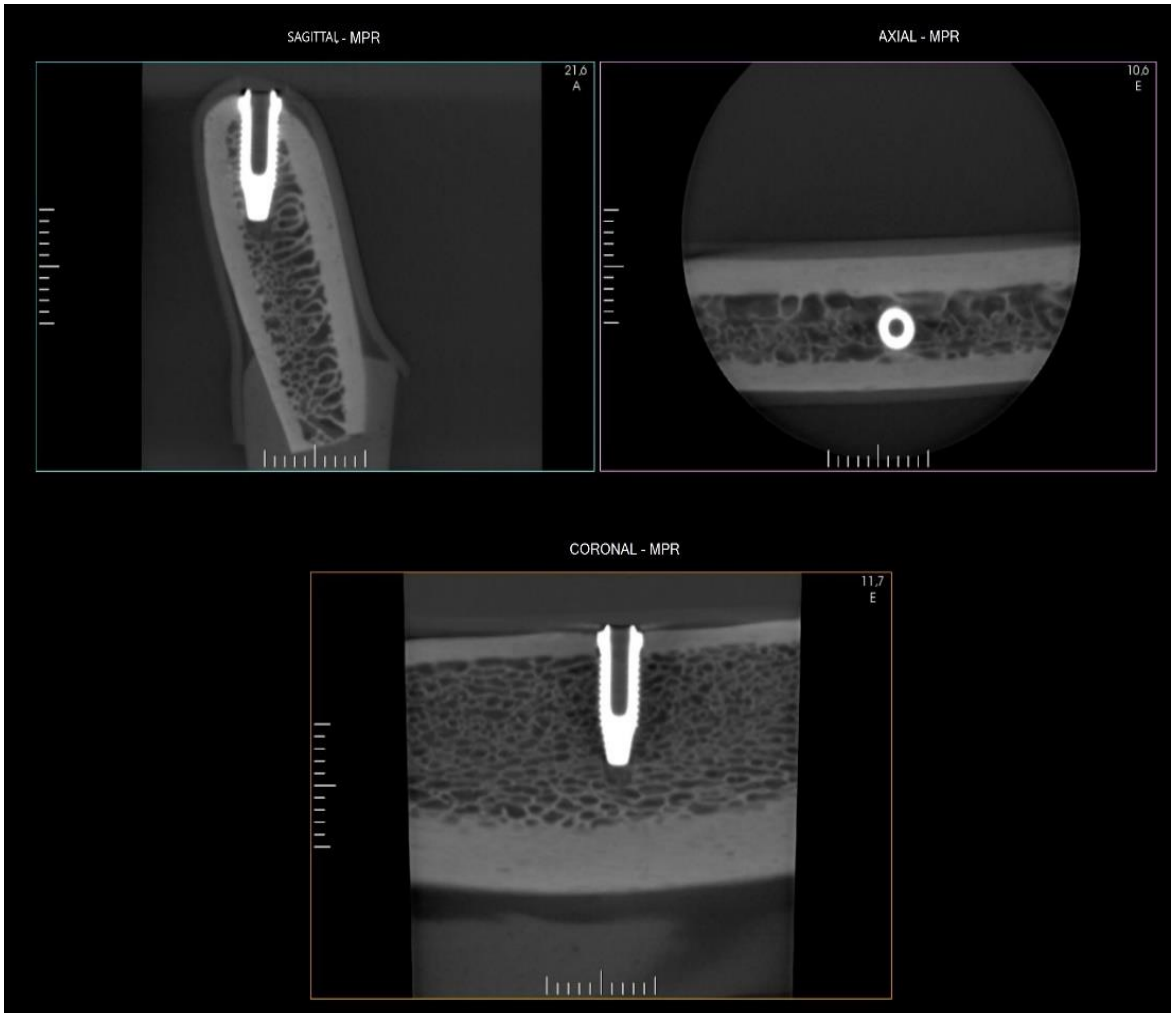

Source: Author.

Figure 2: Sagittal, axial, and coronal reconstructions of the 1-wall bone defect group.

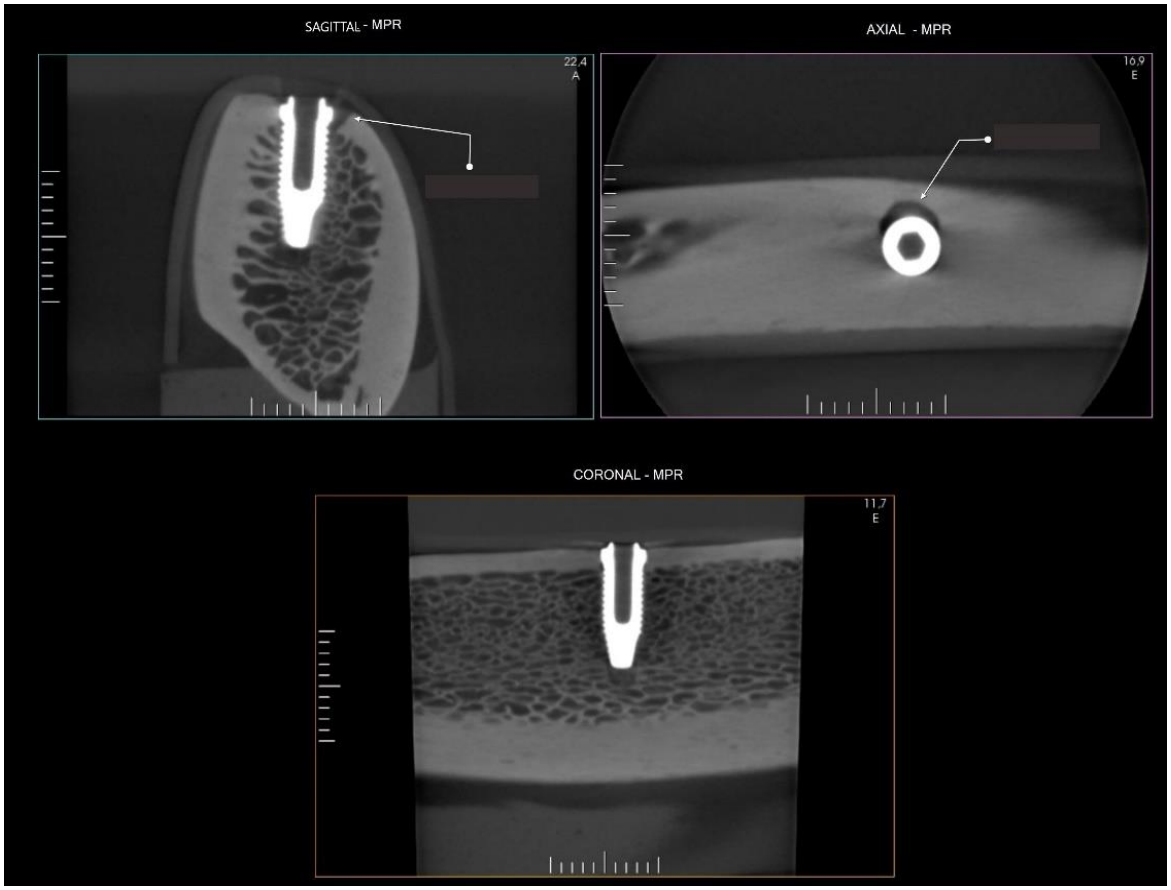

Source: Author.

Figure 3: Sagittal, axial, and coronal reconstructions of the 2-wall bone defect group.

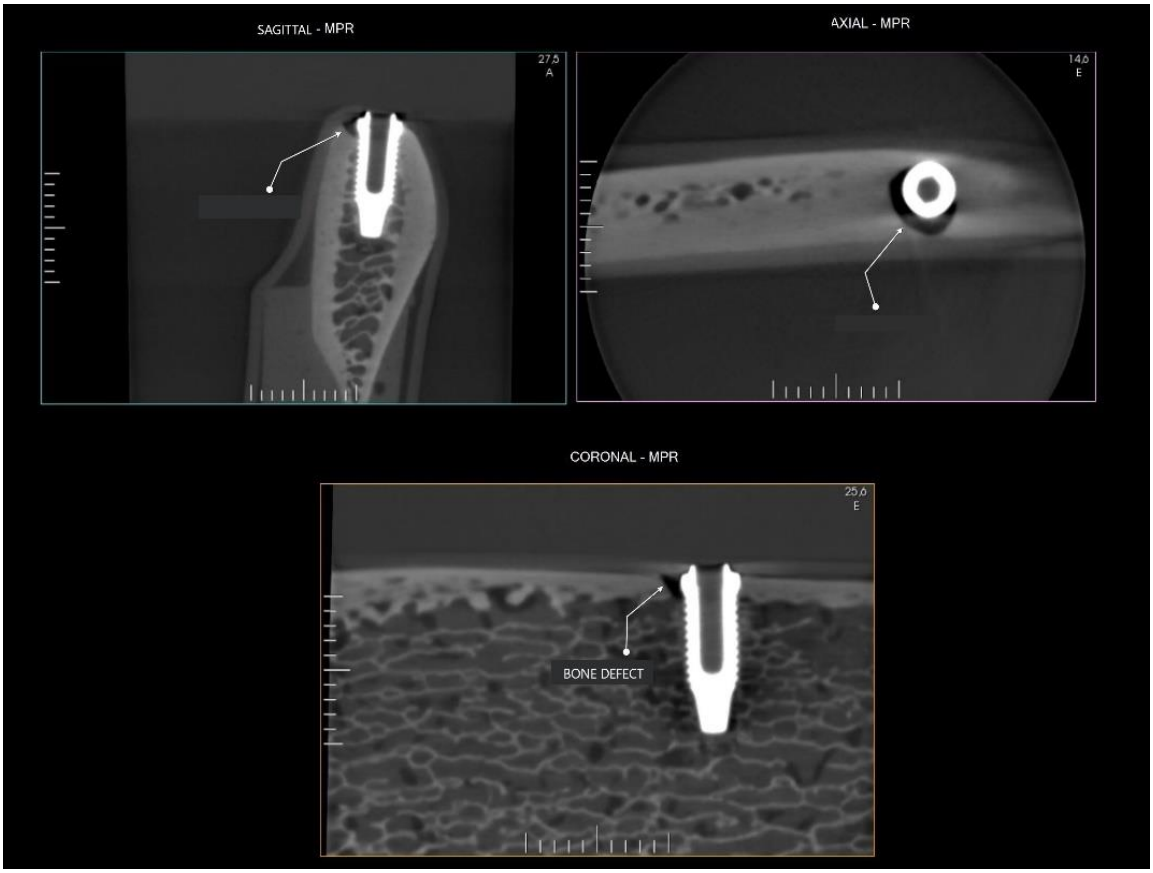

Source: Author.

Figure 4: Sagittal, axial, and coronal reconstructions of the 3-wall bone defect group.

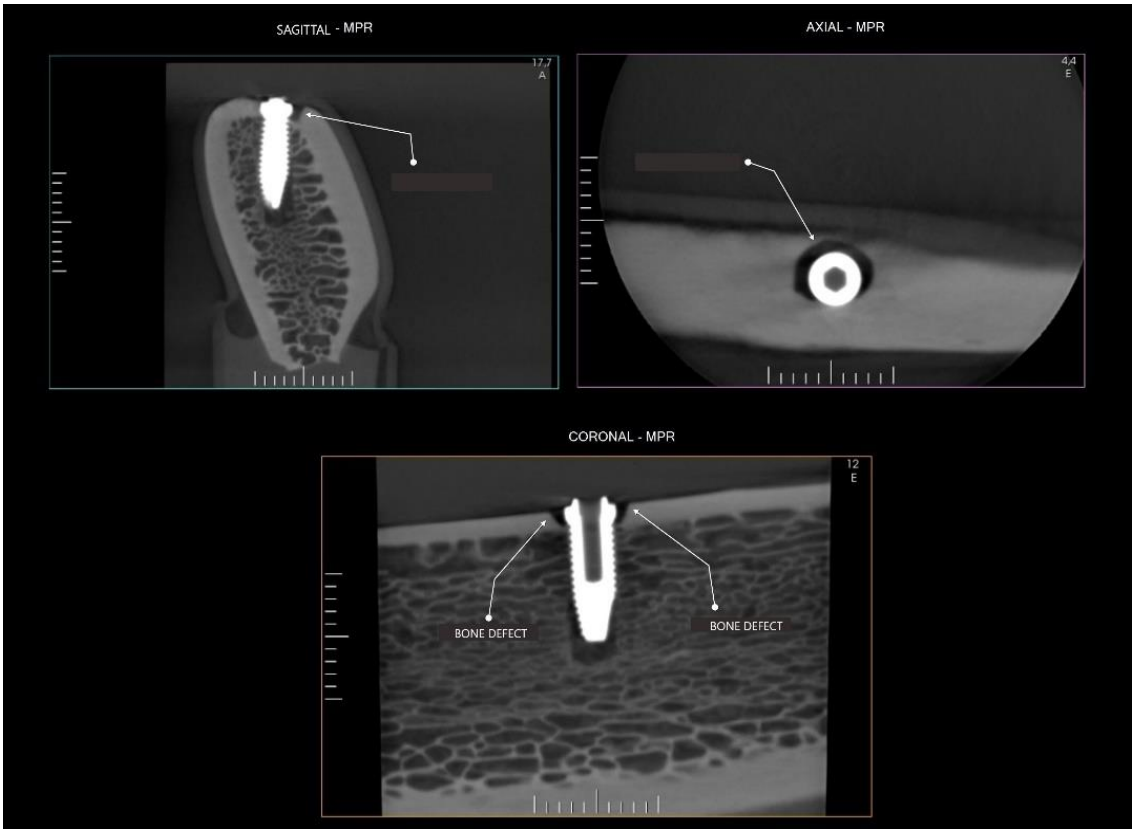

Source: Author.

Figure 5: Sagittal, axial, and coronal reconstructions of the 4-wall bone defect group.

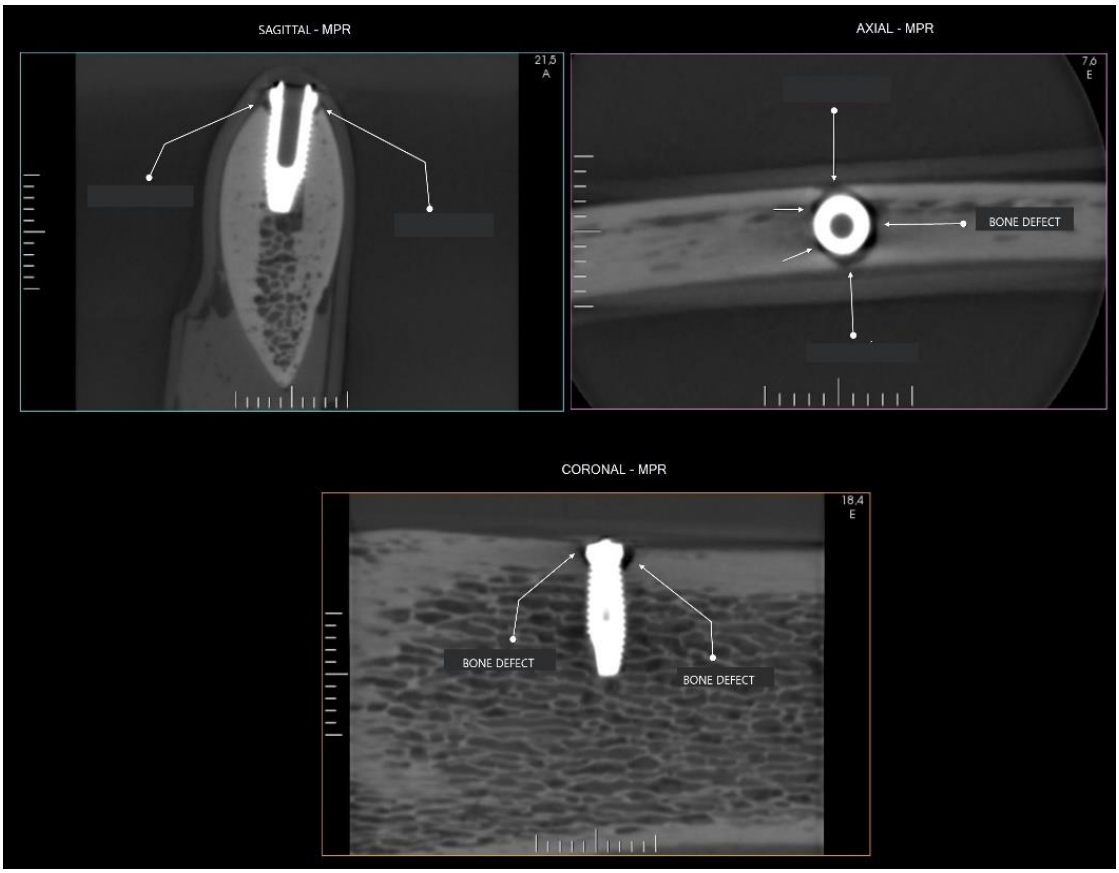

Source: Author.

To evaluate the correct identification of bone defect presence and type across the four protocols, an agreement test was performed. To classify the level of agreement between the actual defect type and the evaluation from each device, the benchmarks proposed by Altman (1991) for Cohen's Kappa coefficient were used: ≤ 0.20 poor, 0.21 - 0.40 fair, 0.41 - 0.60 moderate, 0.61 - 0.80 good, and 0.81 - 1.00 very good.A análise estatística foi realizada com o programa Statistical Package for the Social Sciences (SPSS), versão 26 para Windows (IBM Corp. Released, 2019).

RESULTS

The results showed correct identification percentages (agreement) for the 12 specimens without defects and the 12 specimens with defects in the evaluations for ProtA1 (correct identification = 100%, Kappa = 1.000), ProtA2 (correct identification = 100%, Kappa = 1.000), and ProtO2 (correct identification = 100%, Kappa = 1.000). For ProtO1, the correct identification percentage was 95.8%, as one specimen without defects was not correctly identified (23 out of 24 specimens). The Kappa coefficient was 0.917 (95% CI: 0.757–1.000), indicating very good agreement. The identification of defect presence across the four acquisition protocols is presented in Table 1.

Table 1: Identification of bone defect presence across the four acquisition protocols.

		Protocols							
		ProtA1		**ProtA2**		**ProtO1**		**ProtO2**	
Defect	**Blocks**	Without BD	With BD	Without BD	With BD	Without BD	With BD	Without BD	With BD
Without BD	12	**12**	0	**12**	0	**11**	1	**12**	0
With BD	12	0	**12**	0	**12**	0	**12**	0	**12**
Kappa coefficient (IC 95%)		**1.000** -		**1.000** -		**0.917** (0.757-1.000)		**1.000** -	
Correct Identification (%)		**100%**		**100%**		**95.8%**		**100%**	

Source: Author.

The evaluation of ProtA1 (Table 2) correctly identified the type of defect in 8 out of 12 specimens (66.7% of cases), as follows: three specimens with one-wall defects and three specimens with two-wall defects, but only one of the three

specimens with three-wall defects and one of the three specimens with four-wall defects. The Kappa coefficient for this analysis was 0.568 (95% CI: 0.244, 0.891), indicating moderate agreement between the actual defect type and the ProtA1 evaluation.

Table 2: Identification of bone defect in the ProtO1.

		ProtO1				
Defect	**Blocks**	Visible BD, but unclassifiable	1 wall BD	2 wall BD	3 wall BD	4 wall BD
1 wall BD	3	0	**3**	0	0	0
2 wall BD	3	0	0	**3**	0	0
3 wall BD	3	0	0	0	**1**	**2**
4 wall BD	3	**1**	**1**	0	0	**1**
Total	12	**Kappa coefficient = 0.568** (IC95%: 0.244, 0.891) **Correct Identification (%) = 66.7%** (8 em 12)				

Source: Author.

Regarding ProtA2 (Table 3), the percentage of correct identification for the bone defect was 58.3% (7 out of 12 specimens). Of the specimens for each bone defect, two with one-wall defects, three with two-wall defects, and two with three-wall defects were correctly identified, while none with four-wall defects were identified. The Kappa coefficient was 0.500 (95% CI: 0.212, 0.788), indicating moderate agreement between the actual bone defect and the ProtA2 evaluation.

Table 3: Identification of bone defect in ProtA2.

		ProtA2				
Defect	**Blocks**	Visible BD, but unclassifiable	1 wall BD	2 wall BD	3 wall BD	4 wall BD
1 wall BD	3	**1**	**2**	0	0	0
2 wall BD	3	0	0	**3**	0	0
3 wall BD	3	0	0	0	**2**	**1**
4 wall BD	3	**3**	0	0	0	**0**
Total	12	**Kappa coefficient = 0.500** (IC95%: 0.212, 0.788) **Correct Identification (%) = 58.3%** (7 em 12)				

Source: Author.

For the evaluation of ProtO1 (Table 4), the bone defect was correctly identified in 9 out of 12 specimens, corresponding to 75.0% of cases. All three specimens with

one-wall defects, all three with two-wall defects, and all three with three-wall defects were correctly identified; however, identification failed for all three specimens with four-wall defects. The Kappa coefficient was 0.676 (95% CI: 0.397, 0.954), demonstrating good agreement between the actual bone defect and the ProtO1 evaluation.

Table 4: Identification of bone defect in ProtO1**.**

Defect	Blocks	ProtO1				
		Visible BD, but unclassifiable	1 wall BD	2 wall BD	3 wall BD	4 wall BD
1 wall BD	3	0	**3**	0	0	0
2 wall BD	3	0	0	**3**	0	0
3 wall BD	3	0	0	0	**3**	0
4 wall BD	3	**1**	0	0	**2**	**0**
Total	12	**Kappa coefficient = 0.676** (IC95%: 0.397, 0.954) **Correct Identification (%) = 75.0%** (9 em 12)				

Source: Author.

Regarding the evaluation of ProtO2 (Table 5), the percentage of correctly identified bone defects was 75.0% (9 out of 12). Two of the three specimens with one-wall defects, all three with two-wall defects, all three with three-wall defects, and only one of the three with four-wall defects were correctly identified. The Kappa coefficient of 0.684 (95% CI: 0.403, 0.965) indicates good agreement between the actual bone defect and the ProtO2 evaluation.

Table 5: Identification of bone defect in ProtO2.

Defect	Blocks	ProtO2				
		Visible BD, but unclassifiable	1 wall BD	2 wall BD	3 wall BD	4 wall BD
1 wall BD	3	**1**	**2**	0	0	0
2 wall BD	3	0	0	**3**	0	0
3 wall BD	3	0	0	0	**3**	0
4 wall BD	3	**1**	0	**1**	0	**1**
Total	12	**Kappa coefficient = 0.684** (IC95%: 0.403, 0.965) **Correct Identification (%) = 75.0%** (9 em 12)				

Source: Author.

DISCUSSION

Early detection of marginal bone loss is vital for treatment planning and implant prognosis (Song et al, 2021). Tomographic acquisition protocols can influence the reduction of artifact incidence and improve image quality in peri-

implant structures (Sawicki et al, 2022). This study evaluated the influence of CBCT acquisition protocols on the identification of angular bone defects in the cervical area of implants. In general, both devices used allowed for the correct identification of the presence of angular bone defects, with differences occurring only in the identification of the bone defect (1, 2, 3, or 4 walls). The tomographic acquisition protocol did not influence the evaluation of defect types for Protocol O. In contrast, for Protocol A, ProtA1 - with a higher dose (higher resolution) – allowed superior visualization and better results in detecting peri-implant angular bone defects (1, 2, 3, or 4 walls) when compared to ProtA2.

Although both protocols showed moderate agreement, the difference consisted of the reduction in milliamperage (mA), which, according to Pauwels et al. (2014), can increase image noise. Notably, a satisfactory identification (good agreement) was observed for the reliable and reproducible quantification of peri-implant angular bone loss regarding the defect type, regardless of the radiation dose or acquisition protocol. Therefore, the dose protocol did not influence the detection of the affected walls. Consequently, the use of the standard protocol (STD) is recommended, following the ALARA (As Low As Reasonably Achievable) (Nomier et al, 2022), ALADA (As Low As Diagnostically Acceptable), and ALADAIP (As Low As Diagnostically Acceptable, being Indication-oriented and Patient-specific) principles (Oenning et al, 2021).

Regarding acquisition factors, a value equal to or greater than 90 kVp is suggested, as it results in a higher contrast-to-noise ratio (Pauwels et al, 2014) and reduces artifacts such as beam hardening (Sawicki et al, 2022). This corroborates the findings of Pinheiro et al. (2017), where a higher kVp showed a higher detection rate for both small and large peri-implant bone defects. Based on this information, values above 90 kVp were used in both acquisition protocols (Protocol O and Protocol A).

When absorbing X-ray beams, titanium dental implants can cause artifacts in the tomographic image, which originate from three elementary sources: photon starvation, scattering, and beam hardening (Ballhausen et al, 2014), leading to higher gray values in the interproximal area (Jaju et al, 2013; Parsa et al, 2014). Artifacts originating from implants are characterized by hyperdense lines that spread horizontally, known as streak artifacts (Kamburoglu et al, 2013). By generating higher gray values and dark zones in the interproximal area, a non-existent bone defect may be simulated, leading to diagnostic inaccuracy (Costa et al, 2023; Kamburoglu et al, 2013). According to Pinheiro et al. (2015), CBCT images compatible with bone defects are characterized by irregular hypodense zones with small

hyperdense areas (trabecular bone), whereas images produced by metal artifacts are more regular and completely hypodense.

The visualization of four-wall defects was difficult to interpret across both devices and acquisition protocols, differing from the study conducted by Chagas et al. (2021). This result may be justified by considering that defects created with spherical burs, which present a dark band similar to that produced by CBCT metal artifacts (Zhang et al, 2021). Other variables that may have influenced were the difficult detection of buccal peri-implant defects (Kamburoglu et al, 2013) and the cortical thinning in this area (Liedke et al, 2017).

The intra-observer agreement analysis showed very good agreement (94.8%) between the initial evaluations and re-evaluations, validating the reliability of the evaluation method and the applied methodology. In the present study, peri-implant bone defects were created using spherical burs, ensuring satisfactory homogeneity and allowing for the standardization of diagnostic performance tests (Kim et al., 2020). Furthermore, bovine rib bone specimens were selected, as they are commonly used in in vitro studies due to their similarity in contour and dimensions to the human mandible, as well as the presence of both cortical and cancellous bone (Schwindling et al, 2019).

A limitation of this study is that it did not account for mandibular angulation during implant insertion, which does not fully replicate the clinical setting. For future studies, it is suggested to include an additional examiner and utilize inter-observer agreement to evaluate equivalence and reliability, in addition to considering mandibular angulation and adapting implant positioning.

CONCLUSION

It can be concluded that tomographic acquisition factors (kV, mA, and FOV), regardless of the device, influence the identification of the bone defect type, but do not affect the visualization of peri-implant angular bone loss.

REFERENCES

AKHESHTEH, V. et al. Efficacy of Periapical Radiography and Three Cone-Beam Computed Tomography Systems for Detection of Peri-Implant Dehiscence Defects: An in- Vitro Study. **Journal of Biomedical Physics and Engineering**, Shiraz, v. 10, n. 6, p. 751-760, dez. 2020. Disponível em: https://doi.org/10.31661/jbpe.v0i0.2008-1162. Acesso em: 20 jun. 2024.

ALTMAN, D. G. **Practical statistics for medical research**. Londres: Chapman and Hall, 1991. Acesso em: 23 nov. 2024.

BALLHAUSEN, H. et al. Post-processing sets of tilted CT volumes as a method for metal artifact reduction. **Radiation Oncology**, Londres, v. 9, n. 1, p. 114, maio 2014. Disponível em: https://doi.org/10.1186/1748-717X-9-114. Acesso em: 20 jun. 2024.

BAYRAK, S. et al. Evaluation of a metal artifact reduction algorithm and in optimization filter in the estimation of peri-implant dehiscence defects by using cone beam computed tomography: an in-vitro study. **Oral Surgery, Oral Medicine, Oral Pathology, Oral Radiology**, St. Louis, v. 130, n. 2, p. 209-216, ago. 2020. Disponível em: https://doi.org/10.1016/j.oooo.2020.02.005. Acesso em: 20 jun. 2024.

CHAGAS, M. M. et al. Diagnostic accuracy of imaging examinations for peri-implant bone defects around titanium and zirconium dioxide implants: A systematic review and meta-analysis. **Imaging Science in Dentistry**, Seul, v. 51, n. 4, p. 363-372, dez. 2021. Disponível em: https://doi.org/10.5624/isd.20210120. Acesso em: 20 jun. 2024.

COSTA, J. A. et al. Analysis of peri-implant bone defects by using cone beam computed tomography (CBCT): an integrative review. **Oral Radiology**, Tóquio, v. 39, n. 3, p. 455-466, jul. 2023. Disponível em: https://doi.org/10.1007/s11282-023-00683-w. Acesso em: 20 jun. 2024.

DAVE, M. et al. A comparison of cone beam computed tomography and conventional periapical radiography at detecting peri-implant bone defects. **Clinical Oral Implants Research**, Copenhague, v. 24, n. 6, p. 671-678, jun. 2013. Disponível em: https://doi.org/10.1111/j.1600-0501.2012.02473.x. Acesso em: 20 jun. 2024.

FIENITZ, T. et al. Accuracy of cone beam computed tomography in assessing peri-implant bone defect regeneration: a histologically controlled study in dogs. **Clinical Oral Implants Research**, Copenhague, v. 23, n. 7, p. 882-887, jul. 2012. Disponível em: https://doi.org/10.1111/j.1600-0501.2011.02232.x. Acesso em: 20 jun. 2024.

IBM CORP. **IBM SPSS Statistics for Windows**: Version 26.0. Armonk, NY: IBM Corp, 2019. Acesso em: 23 nov. 2024.

JAJU, P. P. et al. Artefacts in cone beam CT. **Open Journal of Stomatology**, Wuhan, v. 3, n. 5, p. 292-297, set. 2013. Disponível em: https://doi.org/10.4236/ojst.2013.35049. Acesso em: 20 jun. 2024.

JALALUDDIN, M. et al. Radiographic Assessment of the Marginal Bone Loss Around the Implant Before and After the Prosthesis Placement-A Comparative Study. **Journal of Pharmacy and Bioallied Sciences**, Mumbai, v. 16, n. 5, p. S4693-S4696, dez. 2024. Disponível em: https://doi.org/10.4103/jpbs.jpbs_1184_24. Acesso em: 20 jun. 2024.

KAMBUROGLU, K. et al. Assessment of buccal marginal alveolar peri-implant and periodontal defects using a cone beam CT system with and without the application of metal artefact reduction mode. **Dentomaxillofacial Radiology**, Londres, v. 42, n. 8, p. 20130176, ago. 2013. Disponível em: https://doi.org/10.1259/dmfr.20130176. Acesso em: 20 jun. 2024.

KIM, J. H. et al. Comparison between different cone-beam computed tomography devices in the detection of mechanically simulated peri-implant bone defects. **Imaging Science in Dentistry**, Seul, v. 50, n. 2, p. 133-139, jun. 2020. Disponível em: https://doi.org/10.5624/isd.2020.50.2.133. Acesso em: 20 jun. 2024.

KUHL, S. et al. Detection of peri-implant bone defects with different radiographic techniques – a human cadaver study. **Clinical Oral Implants Research**, Copenhague, v. 27, n. 5, p. 529–534, maio 2016. Disponível em: https://doi.org/10.1111/clr.12619. Acesso em: 20 maio 2026.

LIEDKE, G. S. et al. Factors affecting the possibility to detect buccal bone condition around dental implants using cone beam computed tomography. **Clinical Oral Implants Research**, Copenhague, v. 28, n. 9, p. 1082-1088, set. 2017. Disponível em: https://doi.org/10.1111/clr.12921. Acesso em: 20 jun. 2024.

NOMIER, A. S. et al. Efficacy of low-dose cone beam computed tomography and metal artifact reduction tool for assessment of peri-implant bone defects: an in vitro study. **BMC Oral Health**, Londres, v. 22, n. 1, p. 615, dez. 2022. Disponível em: https://doi.org/10.1186/s12903-022-02663-8. Acesso em: 03 jul. 2024.

OENNING, A. C. et al. ALADAIP, beyond ALARA and towards personalized optimization for paediatric cone-beam CT. **International Journal of Paediatric Dentistry**, [S. l.], v. 31, n. 5, p. 676-678, set. 2021. Disponível em: https://doi.org/10.1111/ipd.12797. Acesso em: 03 jul. 2025.

PARSA, A. et al. Assessment of metal artefact reduction around dental titanium implants in cone beam CT. **Dentomaxillofacial Radiology**, Londres, v. 43, n. 7, p. 20140019, set. 2014. Disponível em: https://doi.org/10.1259/dmfr.20140019. Acesso em: 03 jul. 2025.

PAUWELS, R. et al. A pragmatic approach to determine the optimal kVp in cone beam CT: balancing contrast-to-noise ratio and radiation dose. **Dentomaxillofacial Radiology**, Londres, v. 43, n. 5, p. 20140059, maio 2014. Disponível em: https://doi.org/10.1259/dmfr.20140059. Acesso em: 03 jul. 2025.

PINHEIRO, L. R. et al. Effect of field of view in the detection of chemically created peri-implant bone defects in bovine ribs using cone beam computed tomography: an in vitro study. **Oral Surgery, Oral Medicine, Oral Pathology, Oral Radiology**, St. Louis, v. 120, n. 6, p. 780, dez. 2015. Disponível em: https://doi.org/10.1016/j.oooo.2015.04.006. Acesso em: 03 jul. 2025.

PINHEIRO, L. R. et al. Effectiveness of Periapical Radiography Versus Cone Beam Computed Tomography with Different Kilovoltage Settings in the Detection of Chemically Created Peri-implant Bone Defects: An In Vitro Study. **International Journal of Oral & Maxillofacial Implants**, Chicago, v. 32, n. 4, p. 741-750, ago. 2017. Disponível em: https://doi.org/10.11607/jomi.5311. Acesso em: 03 jul. 2025.

SALEMI, F. et al. Efficacy of Metal Artifact Reduction Algorithm of Cone-Beam Computed Tomography for Detection of Fenestration and Dehiscence around Dental Implants. **Journal of Biomedical Physics and Engineering**, Shiraz, v. 11, n. 3, p. 305-314, jun. 2021. Disponível em: https://doi.org/10.31661/jbpe.v0i0.2102-1284. Acesso em: 03 jul. 2025.

SANZ-MARTÍN, I. et al. Factors associated with the presence of peri-implant buccal soft tissue dehiscences. **Clinical Oral Implants Research**, Copenhague, v. 31, n. 4, p. 344-354, abr. 2020. Disponível em: https://doi.org/10.1111/clr.13572. Acesso em: 20 maio 2026.

SAWICKI, P. et al. Influence of Exposure Parameters and Implant Position in Peri-Implant Bone Assessment in CBCT Images: An In Vitro Study. **Journal of Clinical Medicine**, Basileia, v. 11, n. 13, p. 3846, jul. 2022. Disponível em: https://doi.org/10.3390/jcm11133846. Acesso em: 03 jul. 2025.

SAWICKI, P. et al. The Impact of Cone-Beam Computed Tomography Exposure Parameters on Peri-Implant Artifacts: A Literature Review. **Cureus**, São Francisco, v. 14, n. 3, p. e23035, mar. 2022. Disponível em: https://doi.org/10.7759/cureus.23035. Acesso em: 03 jul. 2025.

SCHRIBER, M. et al. Cone beam computed tomography artefacts around dental implants with different materials influencing the detection of peri-implant bone defects. **Clinical Oral Implants Research**, Copenhague, v. 31, n. 7, p. 595-606, jul. 2020. Disponível em: https://doi.org/10.1111/clr.13596. Acesso em: 03 jul. 2025.

SCHWINDLING, F. S. et al. In vitro diagnostic accuracy of low-dose CBCT for evaluation of peri-implant bone lesions. **Clinical Oral Implants Research**, Copenhague, v. 30, n. 12, p. 1200-1208, dez. 2019. Disponível em: https://doi.org/10.1111/clr.13533. Acesso em: 03 jul. 2025.

SONG, D. et al. Diagnostic accuracy of CBCT versus intraoral imaging for assessment of peri-implant bone defects. **BMC Medical Imaging**, Londres, v. 21, n. 1, p. 23, fev. 2021. Disponível em: https://doi.org/10.1186/s12880-021-00557-9. Acesso em: 03 jul. 2025.

VADIATI SABERI, B. et al. Detection of peri-implant bone defects using cone-beam computed tomography and digital periapical radiography with parallel and oblique projection. **Imaging Science in Dentistry**, Seul, v. 49, n. 4, p. 265-272, dez. 2019. Disponível em: https://doi.org/10.5624/isd.2019.49.4.265. Acesso em: 02 fev. 2023.

ZHANG, C. N. et al. Intra- and inter-observer agreements in detecting peri-implant bone defects between periapical radiography and cone beam computed tomography: A clinical study. **Journal of Dental Sciences**, Amsterdã, v. 16, n. 3, p. 948-956, jul. 2021. Disponível em: https://doi.org/10.1016/j.jds.2020.10.013. Acesso em: 03 jul. 2025.